

Development of a SiC detector array within the SAMOTHRACE ecosystem

N. S. MARTORANA^{(1)(*)}, G. D'AGATA⁽¹⁾⁽²⁾, A. BARBON⁽¹⁾⁽²⁾, G. CARDELLA⁽¹⁾,
E. GERACI⁽¹⁾⁽²⁾⁽³⁾, L. ACOSTA⁽⁴⁾⁽⁵⁾, C. ALTANA⁽⁶⁾, A. CASTOLDI⁽⁷⁾,
E. DE FILIPPO⁽¹⁾, S. DE LUCA⁽⁶⁾, B. GNOFFO⁽¹⁾⁽²⁾, C. GUAZZONI⁽⁷⁾,
C. MAIOLINO⁽⁶⁾, E. V. PAGANO⁽⁶⁾, S. PIRRONE⁽¹⁾, G. POLITI⁽¹⁾⁽²⁾,
L. QUATTROCCHI⁽¹⁾⁽⁸⁾, F. RISITANO⁽¹⁾⁽⁸⁾, F. RIZZO⁽²⁾⁽³⁾⁽⁶⁾, P. RUSSOTTO⁽⁶⁾,
G. SAPIENZA⁽⁶⁾, M. TRIMARCHI⁽¹⁾⁽⁸⁾, S. TUDISCO⁽⁶⁾ and C. ZAGAMI⁽²⁾⁽³⁾⁽⁶⁾

⁽¹⁾ INFN, Sezione di Catania - Catania, Italy

⁽²⁾ Dipartimento di Fisica e Astronomia "Ettore Majorana", Università degli Studi di Catania Catania, Italy

⁽³⁾ CSFNSM - Catania, Italy

⁽⁴⁾ Instituto de Física, Universidad Nacional Autónoma de México - Mexico City, Mexico

⁽⁵⁾ Instituto de Estructura de la Materia, CSIC - Madrid, Spain

⁽⁶⁾ INFN-LNS - Catania, Italy

⁽⁷⁾ DEIB Politecnico Milano and INFN, Sezione di Milano - Milano, Italy

⁽⁸⁾ Dipartimento MIFT, Università di Messina - Messina, Italy

received 26 November 2024

Summary. — In recent years, the scientific community has shown an increasing interest in utilizing SiC-based particle detectors, particularly for investigations in nuclear and medical physics. This growing interest is driven largely by the remarkable properties of SiC, combined with advancements in device fabrication techniques. Within the SAMOTHRACE ecosystem—which focuses also on developing new-generation SiC-based detectors—significant progress has been made in characterizing these detectors for their use in both medical and nuclear physics. This contribution presents some of the key results obtained from this characterization process by means of first tests using radioactive α sources.

1. – Introduction

Silicon carbide (SiC) material exhibits numerous characteristics that make it an excellent candidate as a charged-particle detector. Among these, its wide band gap allows for low noise and visible-light blindness, its high electron saturation velocity enables a fast signal response, its high displacement energy is synonymous with radiation hardness, and its high thermal conductivity facilitates heat dissipation [1, 2]. Among these various properties, radiation hardness is particularly noteworthy for two key reasons. The first one is its relevance for nuclear physics. Currently, several facilities are either in construction or in upgrading for producing high-intensity stable and radioactive beams, with the

(*) E-mail: nunzia.martorana@ct.infn.it

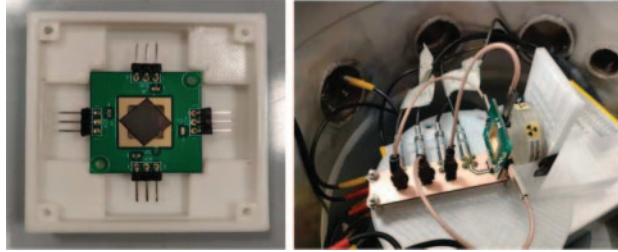


Fig. 1. – (Color online). Left: picture of 2×2 pads SiC detector, with a thickness of $100 \mu\text{m}$ and a surface of 1cm^2 . Right: picture of the mixed α source placed in front of the SiC detector.

primary goal of studying reactions with low cross-sections or reactions involving nuclei far from the stability valley [3-6]. The second reason pertains to medical physics, where the use of SiC dosimeters, micro-dosimeters, and beam monitors within the hadron therapy technique could significantly improve the clinical approaches [7]. Within the SAMOTH-RACE ecosystem, specifically in the context of WP4, Spoke 5, SiC detectors are being developed [8]. The main aim of this work is to have a portable, compact, and versatile SiC array detector usable in several facilities worldwide for both nuclear and medical investigations, even in the case of high-intensity radioactive ion beams (RIBs). In particular, among RIBs, ^{11}C have been identified as promising ions for improving the hadron therapy technique. This is due to their decay properties, which can be utilized for performing imaging, and their high biological effectiveness. These two phenomena could provide an improvement compared to the use of stable ions, such as ^{12}C [9-11]. Some tests have been performed using such ions, studying their production and interaction with biological material, with the aim of mimicking the interaction and the deposited dose in human body [9-11]. Among the various facilities worldwide, the FraISE one, currently under construction at INFN-LNS, in Catania, offers numerous opportunities for producing and studying high-intensity radioactive ion beams [3, 12-17]. For this specific goal, an array of SiC detectors with high performances in terms of spatial granularity, energy and time resolutions will be used as a tagging/diagnostic element for RIBs produced by FraISE [3, 17]. By using this array, several studies in the field of nuclear physics, ranging from isospin physics, clustering and collective mode investigations, will be conducted, also using the high-performances of the CHIMERA, FARCOS and NARCOS multidetectors [18-26].

In the following section, some experimental results obtained in the characterization of new-generation SiC detectors will be discussed. This work is made possible thanks to the synergy between the CHIRONE Collaboration [27] and the SAMOTH-RACE ecosystem, (pillar Health: SPOKE 5) [8]. Some further results on this SiC characterization, obtained with both simulations and tests, are presented in the contributions to these proceedings by Barbon and D'Agata [28, 29].

2. – Results obtained with radioactive α sources

In this section, results obtained in the characterization of the first 2×2 pads, $100 \mu\text{m}$, 1cm^2 , SiC prototypes are discussed. The first tests have been performed at INFN-LNS, using a mixed α source. For such purpose, a Mesytec preamplifier, MPR 16 channels, and a CAEN digitizer DT5742, set with a frequency of 1 GHz, have been used. Figure 1(left) shows a picture of the 2×2 pads SiC detector. Figure 1(right) shows a picture of

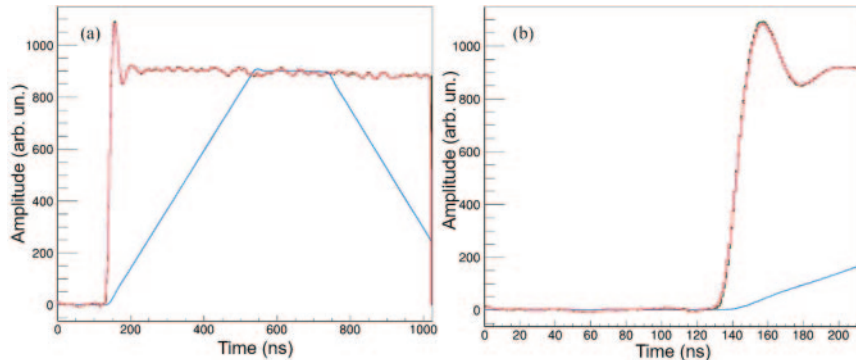


Fig. 2. – (Color online). (a) Blue line: SiC waveform obtained using a mixed α source in vacuum. Azure line: applied trapezoidal filter used to extract the maximum. Pink line: smoothed filter used to extract the timing information, such as rise time and crossing time. (b) Zoomed view for the channels region between 0 and 200 of the figure shown in the left panel.

the α mixed source placed in front of the detector. Using the CAEN digitizer, the signal waveforms have been acquired. As an example, fig. 2(a) —blue line— shows the waveform of an α signal obtained from a SiC pad, while the azure line represents the applied trapezoidal filter, which allows for extracting the maximum and provides information about the energy. Furthermore, a filter able to perform the smoothing of the signal waveform and shown as the pink line in fig. 2(a), enables to extract information about the rise time and the crossing time —also called start time— which is evaluated as the 10% of the extracted maximum. Figure 2(b) displays a zoomed view of fig. 2(a), for the channels in the region between 0 and 200. Figure 3(a) shows the calibrated energy *vs.* rise time plot obtained for a SiC pad. Some events with a higher rise time ($\approx > 7$ ns) and lower energy are present. These events are primarily (99%) associated with multiplicity = 1, while a smaller percentage is due to events with multiplicity = 2. Such events are probably due to an edge effect, where charge collection is less efficient compared to the center of the detector. Figure 3(b) shows the calibrated energy spectrum obtained for a SiC pad. This spectrum was obtained with a cut for multiplicity = 1 and by removing events with rise time > 7 ns. Performing Gaussian fits, an energy resolution of ≈ 51 keV was obtained. Some data analysis, simulations, and tests are ongoing to clarify the reasons for these events with lower rise time as well as to improve the obtained energy resolution. The simulations performed are discussed in the contribution of D’Agata to these proceedings [29]. A similar analysis has been performed using a 2×2 pads $10 \mu\text{m}$ thick- 1 cm^2 SiC detector, which is discussed by Barbon in these proceedings [28].

Using the mixed α source, a preliminary investigation on the timing performances of these new-generation silicon carbide detectors has been performed, looking at the sharing signals, *i.e.*, signals in events in which two adjacent pads are in coincidence. The first test has been performed in air, placing the α mixed source in front of the detector. Figure 4(a) shows the energy of one pad *vs.* the energy of an adjacent pad in coincidence events: three lines are visible that correspond to the three energies of α mixed source. Figure 4(b) shows the time difference between the start/crossing signals of the two pads in coincidence. In particular, fig. 4(b) displays three timing distributions: the blue filled histogram is obtained with a cut in the central energy region of pad₂ (250

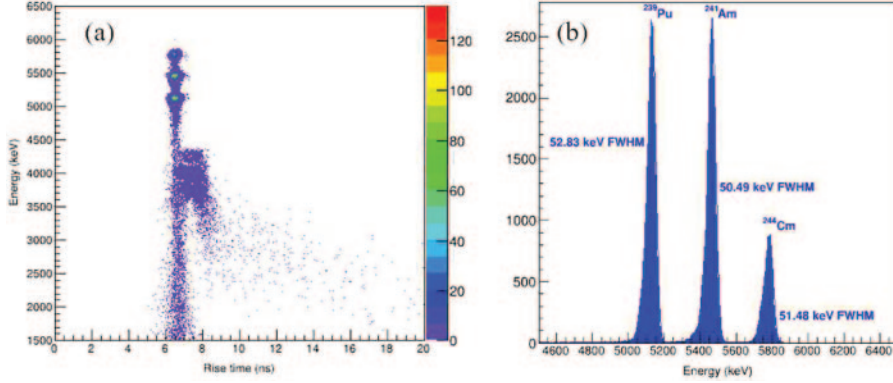


Fig. 3. – (Color online). (a) Energy *vs.* rise time plot obtained using a mixed α source. (b) Calibrated energy spectrum obtained with a cut in multiplicity = 1 and in rise time < 7 ns.

arb.un. < $Energy_{pad_2}$ < 450 arb.un.); the two light and dark green curves are obtained with cuts in the extreme regions of fig. 4(a), *i.e.*, 50 arb.un. < $Energy_{pad_2}$ < 250 arb.un. and 450 arb.un. < $Energy_{pad_2}$ < 650 arb.un., respectively, where the energy of one pad is lower than the energy of the adjacent pad. The observed trend is consistent with expectations. Actually, the timing distribution worsens when the energy of one pad is lower than the energy of the adjacent pad. This is due to the fact that the timing response is more affected by the pad with the lower energy. Along this line, to obtain preliminary information on the detector's timing performance, we focused the data analysis on signals with approximately the same energy in both adjacent pads (250 arb.un. < $Energy_{pad_2}$ < 450 arb.un.), as in the case of blue timing distribution. Further cuts have been included in data analysis: first of all, a cut on the energy of the

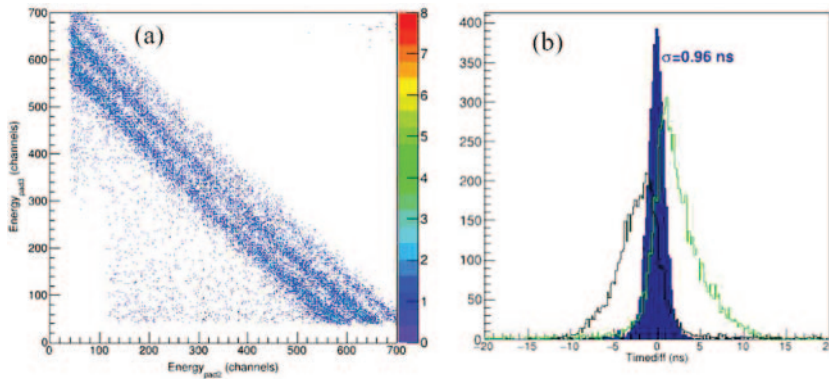


Fig. 4. – (Color online). (a) Energy of a pad *vs.* the energy of an adjacent pad in coincidence events. (b) Timing difference between the crossing signals in coincidence events. In detail the blue filled distribution is obtained with a cut in energy (250 arb.un. < $Energy_{pad_2}$ < 450 arb.un.), the light green distribution is obtained with a cut 50 arb.un. < $Energy_{pad_2}$ < 250 arb.un. and the dark green one is obtained with the cut in energy 450 arb.un. < $Energy_{pad_2}$ < 650 arb.un. The σ value has been obtained performing a Gaussian fit on the blue filled distribution.

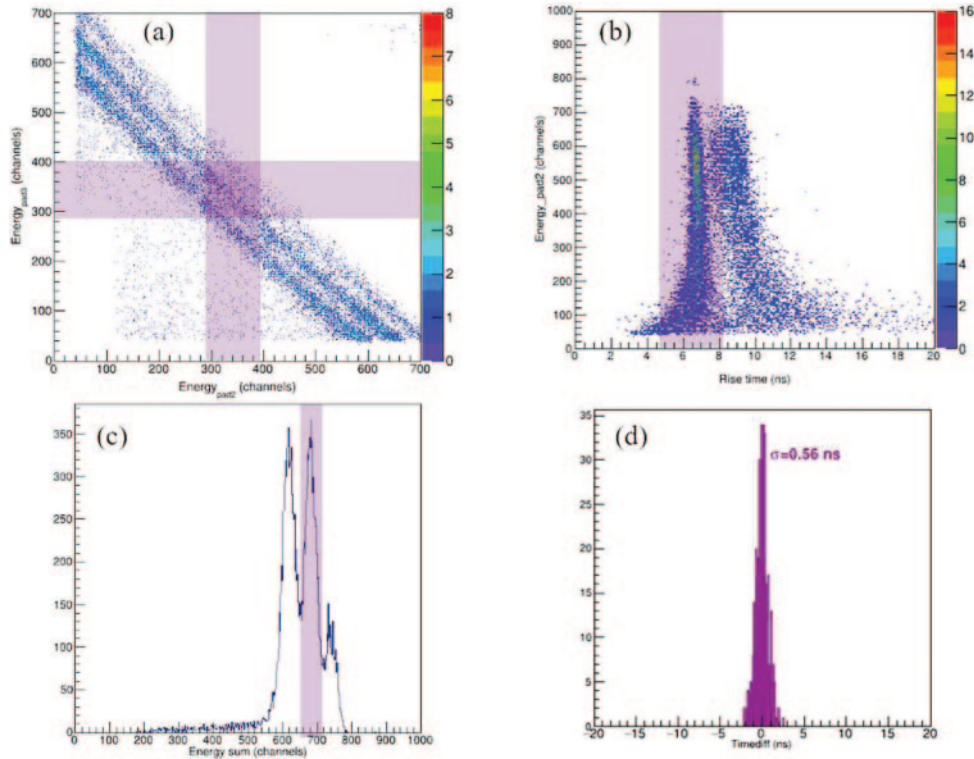


Fig. 5. – (Color online). (a) Energy of a pad *vs.* the energy of an adjacent pad in coincidence events. The violet rectangles indicate the performed cuts. (b) Energy *vs.* rise time plot of one pad in coincidence events with the other pad; the violet region indicates the performed cut, which was applied also for the other pad. (c) Energies sum of two pads in coincidence events; the violet region indicates the performed cut. (d) Timing difference between the start signals obtained with cuts shown in panels (a)–(c) by means of violet regions. σ has been obtained within a Gaussian fit.

second pad (pad_3) was also included to have a narrow selection in energies of two pads, as displayed roughly by means of violet rectangles shown in fig. 5(a); second, a cut on the rise time was included to remove the presence of events due to the edge effect (rise time > 7 ns), as shown in panel (b) of fig. 5; third, a constraint in the sum of the two energies was included, as shown in panel (c) of fig. 5. Figure 5(d) shows the obtained timing distribution with all these cuts. Performing a Gaussian fit, a σ of ≈ 0.6 ns has been obtained. Assuming that pads have the same response in this energy range, the σ_t for each pad is ≈ 0.4 ns.

These preliminary results are very promising and show good performances of the SiC used detector. A further data analysis performed on tests in vacuum and with first protons and α beams is ongoing, to fully characterize these new-generation SiC detectors. In addition, future tests will be devoted to the coupling of SiC prototypes with a fast front-end electronics developed at the INFN Sezione di Milano and Politecnico di Milano [30], and new experiments at the INFN-LABEC of Florence and at the HIL, in Warsaw. Moreover, a production phase of new SiC prototypes has been started.

3. – Conclusions

In this contribution preliminary results obtained in the characterization of new-generation 2×2 pads SiC detectors, $100 \mu\text{m}$, 1 cm^2 , coupled with commercial electronics, and using a mixed α radioactive source have been discussed. The obtained results are promising and show an energy resolution of $\approx 1\%$ in an energy range of $\approx 5 \text{ MeV}$ and a timing resolution with $\sigma_t \approx 0.4 \text{ ns}$ in an energy range of $\approx 2 \text{ MeV}$. Further analysis on measurements performed in vacuum and with first proton and α beams is ongoing. In addition, new results will be obtained with the next tests at the INFN-LABEC of Florence and at the HIL of Warsaw, using protons and carbon beams, respectively. In these latter tests, the detectors will be coupled with a dedicated fast front-end electronics, developed at INFN Sezione di Milano and Politecnico di Milano.

* * *

This work has been partially funded by European Union (NextGeneration EU), through MUR-PNRR project SAMOTHRACE (ECS00000022) and DGAPA-PAPIIT IG101423.

REFERENCES

- [1] TUDISCO S. *et al.*, *Sensors*, **18** (2018) 2289.
- [2] DE NAPOLI M., *Front. Phys.*, **10** (2022) 898833.
- [3] MARTORANA N. S. *et al.*, *Front. Phys.*, **10** (2022) 1058419.
- [4] <https://frib.msu.edu/> (2024).
- [5] AGODI C. *et al.*, *Eur. Phys. J. Plus*, **138** (2023) 1038.
- [6] BALLAND M. *et al.*, *Eur. Phys. J. Plus*, **138** (2023) 709.
- [7] PARISI G., ROMANO F. and SCETTINO G., *Front. Phys.*, **10** (2022) 1035956.
- [8] <https://samothrace.eu/> (2024).
- [9] DURANTE M. and PARODI K., *Front. Phys.*, **8** (2020) 00326.
- [10] BOSCOLO D. *et al.*, *Front. Oncol.*, **11** (2021) 737050.
- [11] KOSTYLEVA D. *et al.*, *Phys. Med. Biol.*, **68** (2022) 015003.
- [12] POTLNS project, <https://potlns.lns.infn.it/> (2022).
- [13] RUSSOTTO P. *et al.*, *J. Phys. Conf. Ser.*, **1014** (2018) 012016.
- [14] RUSSO A. *et al.*, *Nucl. Instrum. Methods B*, **463** (2020) 418.
- [15] MARTORANA N. S., *Nuovo Cimento C*, **44** (2021) 1.
- [16] MARTORANA N. S. *et al.*, *Nuovo Cimento C*, **45** (2022) 63.
- [17] MARTORANA N. S. *et al.*, *Nuovo Cimento C*, **47** (2024) 56.
- [18] BADALÀ A. *et al.*, *Riv. Nuovo Cimento*, **45** (2022) 189.
- [19] PAGANO A. *et al.*, *Eur. Phys. J. A*, **56** (2020) 102.
- [20] GNOFFO B. *et al.*, *Front. Phys.*, **10** (2022) 1061633.
- [21] GERACI E. *et al.*, *Nuovo Cimento C*, **45** (2022) 44.
- [22] RISITANO F. *et al.*, *Nuovo Cimento C*, **45** (2022) 60.
- [23] MARTORANA N. S. *et al.*, *Phys. Lett. B*, **782** (2018) 112.
- [24] PAGANO E. V. *et al.*, *EPJ Web of Conferences*, **117** (2016) 10008.
- [25] PAGANO E. V. *et al.*, *Front. Phys.*, **10** (2023) 1051058.
- [26] PAGANO E. *et al.*, *Nucl. Instrum. Methods Phys. Res. A*, **1064** (2024) 169425.
- [27] <https://web.infn.it/CHIMERA/index.php/it/> (2024).
- [28] BARBON A. *et al.*, these proceedings.
- [29] D'AGATA G. *et al.*, these proceedings.
- [30] CASTOLDI A. *et al.*, *IEEE Trans. Nucl. Sci.*, **70** (2023) 1431.